J Clust Sci (2017) 28:1647–1665
DOI 10.1007/s10876-017-1178-0

ORIGINAL PAPER

Application of Gold(III) Acetate as a New Precursor for the Synthesis of Gold Nanoparticles in PEG Through Ultrasonic Spray Pyrolysis

Mohammed Shariq[1,2] · Peter Majerič[1] · Bernd Friedrich[3] · Bojan Budic[4] · Darja Jenko[5] · Amit Rai Dixit[2] · Rebeka Rudolf[1,6]

Received: 1 December 2016 / Published online: 8 February 2017

Abstract The present investigation reports the first-time successful synthesis of AuNPs using a new precursor salt of Au(III) acetate through USP. An aqueous solution of this salt was prepared with very limited solubility with H_2O. HCl and HNO_3 were then added separately to increase the solubility, resulting in a clear, yellowish solution. This enabled the successful formation of AuNPs with USP. In order to improve AuNPs synthesis, NaOH and Na_2CO_3 were added into the precursor to increase its pH (6–7). With such approach, it was possible to perform USP synthesis using varying concentrations of [Au] in the precursor. Evaporation and reaction temperatures (100 and 300 °C) of USP were chosen based on detected decomposition temperatures of Au(III) acetate with TGA-DT. TEM confirmed the presence of circular shaped, unagglomerated AuNPs having an Fm-3m space group with diameter range of 15–30 and circularity value range of 0.89–0.92. The UV–Vis spectroscopy showed absorbance peaks at 528 and 532 nm. ICP-MS indicated the highest concentration of AuNPs, 79 ppm, by the precursor with the lower initial concentration of [Au]. This could be due to the smallest sedimentation and turbulent losses of larger AuNPs in transport tubes and reaction USP zones.

✉ Mohammed Shariq
mohdshariq.03@hotmail.com

[1] Institute of Materials Technology, University of Maribor, 2000 Maribor, Slovenia

[2] Indian Institute of Technology (Indian School of Mines), Dhanbad, Jharkhand 826004, India

[3] IME Institute, RWTH Aachen, 52056 Aachen, Germany

[4] National Institute of Chemistry, 1000 Ljubljana, Slovenia

[5] Institute of Metals and Technology, 1000 Ljubljana, Slovenia

[6] Zlatarna Celje d.d., 3000 Celje, Slovenia

Keywords Au(III) acetate · Ultrasonic spray pyrolysis · Gold nanoparticles · Insolubility · Circular · Unagglomerated

Abbreviations

AuNPs	Gold nanoparticles
USP	Ultrasonic spray pyrolysis
Au(III) acetate	Gold(III) acetate
TGA-DT	Thermal gravimetric analysis—differential thermal
MO_x	Metal oxide powder
TEM	Transmission electron microscopy
UV–Vis	Ultraviolet visible
SPR	Surface plasmon resonance
PEG	Polyethylene glycol
PVP	Polyvinylpyrrolidone
BSA	Bovine serum albumin
wt%	Weight percent
RES	Reticuloendothelial system
EDX	Energy-dispersive X-ray spectroscopy
DLS	Dynamic light scattering
FCC	Face centered cubic
ICP-OES	Optical emission spectroscopy with inductively coupled plasma mass
FTIR	Fourier transform infrared spectroscopy
SD	Standard deviation
fg	Femto gram (10^{-15})

Introduction

Gold nanoparticles (AuNPs) in spherical shape are one of the promising candidates for application in the field of Biotechnology (e.g., biosensors [1–4], cell and tissue engineering and open MR imaging) [5, 6], energy (e.g., high K capacitors and solar cells [7]) and Information Technology (e.g., fiber-optic communication systems and printable electronics) [8, 9]. These applications of the colloidal AuNPs have fueled research and advancements in the preparation of monodispersed AuNPs with controllable sizes, diverse morphologies and assorted functionalities [10–12]. The synthesis of AuNPs by thermal decomposition of suitable metal precursors in the liquid phase has received significant attention from the scientific community as a reliable synthetic route to prepare metal NPs of controlled size and shape [13–16].

In the synthesis of a gold catalyst supported by wet methods, hydrogen tetrachloroaurate ($HAuCl_4$) was used mostly as a precursor for producing AuNPs. However, this precursor causes the growth of AuNPs to a size greater than 30 nm, as well as the poisoning of active sites of AuNPs [17]. This increase in AuNPs sizes results in the coalescence and agglomeration of AuNPs and poisoning of actives sites limits their functionality in biomedical applications. Although many attempts

have been made to control these effects from $HAuCl_4$ precursor [18–21], a clear cut answer to this problem is the use of an alternative precursor of gold and, for this, Gold(III) acetate [Au(III) acetate] is a promising candidate. Au(III) and Au(I) were the common oxidation states of gold for AuNPs, but the precursors for the synthesis of AuNPs were based mainly on Au(III) derivatives [22]. Solid phase metal acetate precursors such as Au(III) acetate have shown a tremendous potential to expand the composition and architecture of nanoparticles. The Au(III) acetate was always readily available and its rich chemistry has long been recognized, even though it's low solubility in most solvents limits its use in the synthesis of AuNPs [23]. Therefore, Au(III) acetate being used as a precursor with its inherent characteristic of insolubility in common solvents makes the synthesis process more difficult to investigate in the solution phase. Thus, the synthesis mechanism of AuNPs from Au(III) acetate through USP remains a major challenge and deserves insightful exploration.

Investigation of Au(III) acetate through TGA-DT analysis had also led to clues on how to control the properties of the resulting AuNPs in terms of morphology and phase composition [24]. The decomposition of Au(III) acetate had suggested the formation of acetic acid as the dominant organic by-product when decomposition yields a pure Au metal in the form of AuNPs [25]. Earlier works reported that the Au(III) acetate powder was sonicated in water to form a colloidal solution of Au(III) acetate. Anhydrous sodium bicarbonate was added at the reflux boiling to achieve the pH level at 10–11. A colorless Au(III) solution was synthesized and metal oxide powder (MO_x) was added to this solution through impregnation, calcination (623 K), washing and drying. Thus, the final product obtained was an Au/MO_x catalyst. The Au(III) solution used in the synthesis method contained no chloride anion, no nitrogen compound, such as ammonia and amine, and no sulfur compounds, such as thiols [26].

Ultrasonic spray pyrolysis (USP) is an aerosol technique used widely for the synthesis of different materials, especially metals and metal oxides, and it can lead to the formation of different morphologies [27–32]. It is a continuous flow process that operates at ambient pressure; therefore, it is more economical than other processes (such as sol–gel and chemical vapor deposition) that involves multiple steps or must be conducted under vacuum. The process involves four major steps: Generation of aerosol droplets from a precursor solution through an ultrasonic generator, drop size shrinkage due to evaporation, chemical reaction, and collection of nanoparticles. During the growth of AuNPs, the nucleation process is dominant at higher temperatures due to the relatively higher thermodynamics level and to changes in the crystalline structure. Higher reaction temperatures give larger average particle size, which increases coalescence and the growth of nanoparticles [33]. Nanoparticles exhibit depressed melting points when compared with their bulk counterparts, which is another important factor for interparticle coalescence and growth [34, 35]. This hydrometallurgical based synthesis mechanism provides a direct production route to such revolutionary particles and the range of materials that can be produced has been increased dramatically by diversifying the precursor compounds to include solid phase reactant precursors such as metal acetates [36, 37]

Ultrasonic atomization has the disadvantage of low throughput, but has the advantage of narrow drop size distribution.

Control over particle size and aggregation state in the aerosol can be achieved through judicious selection of process parameters [38–43]. The crystalline phase, degree of oxidation and particle morphology and size are strongly dependent on the synthesis process and, further, the reactant precursor used for the metal nanoparticles [44]. There is a strong relationship between the decomposition properties of the solid phase metal acetate precursors and the product metal/metal oxide nanocomposite materials created during the synthesis of AuNPs [36]. The synthesis of functionalized AuNPs through USP in-between the temperature range of 260 and 500 °C at different ultrasonic frequencies of 2.5 and 0.8 MHz using tetrachloroauric acid were difficult to prepare single shaped AuNPs. Later works in USP showed that the solution properties, such as the precursor composition, concentration and an added reducing agent, may be crucial in order to achieve the desired morphology of AuNPs. The AuNPs in the size range of 50 nm were the most suitable for different bio-medical applications, leading to the best results for cytotoxicity. Modular re-design of the USP showed a better control of the synthesis of AuNPs that led to target final size, spherical morphology and high purity [45–49].

In the reported works of Barreto et al. [50], TEM morphological analysis shows the approximately spherical and nearly mono-dispersed colloidal AuNPs, though a few particles displayed a faceted shape. The UV–Vis spectra of the surface modified AuNPs revealed a shift in SPR peak to a longer wavelength when compared with the original AuNPs. The red shift may be interpreted as changes in the AuNPs' surrounding layer due to the PEG coatings, PVP-coatings and BSA. Tsai et al. [51] performed the experiments with USP and showed the size of the uniform particles decreased as the precursor concentration was reduced. The particle size distribution narrowed very significantly as the precursor concentration decreased from 1.0 to 0.2 wt%. The mean particle declined from 150 to 90 nm and the particle size distribution narrowed significantly as the precursor concentration decreased from 0.5 to 0.01 wt%.

In vivo targeting of AuNPs, PEG has been recommended as a capping material used to provide AuNPs with the requisite stealth against the reticuloendothelial system (RES) which was an essential component of the immune system, composed of phagocytic cells [52]. Several studies have reported that PEG coated AuNPs were successful as image contrast and treatment agents for in vivo targeting [53, 54]. It has been emphasized recently that, if PEG-AuNPs are to have practical application in the field as a biomedical agent, they need a synthesis route with mass production capability [55]. The agglomeration of AuNPs changes the biological traits significantly, as well as the toxicology of AuNPs, and limits their application in several areas of human activity, particularly in the areas of Biomedicine [56–60]. Therefore, PEG has been used as an AuNPs coating agent in our experiments to increase their stability and for further interactions due to its good solubility, biocompatibility and anti-fouling property [61–64]. The stability of colloidal gold is a major obstacle to practical applications, because colloids tend to aggregate in solution. Therefore, PEG will help in protecting the colloids, which will be absorbed

at the AuNPs‘ particle surface, leading to colloids being separated from each other and preventing them from agglomeration [65–67].

The main aim of this work was to find a suitable alternative precursor for controlled synthesis of AuNPs having circular shaped morphology, narrower size distribution and higher concentration with the USP. The current findings in synthesizing AuNPs and the issues faced while using Au(III) acetate as a precursor with USP were reported for the first time with potential solutions that could help the scientific community to use Au(III) acetate with more ease of accessibility. TGA-DT analysis was conducted to study the thermal decomposition of Au(III) acetate that had helped to determine the optimum temperatures for the evaporation and reaction zones. The final series of experiments were conducted by varying the precursor concentrations after some trial runs in USP. Structural properties, morphology, concentration and absorption spectra of the AuNPs coated with PEG-5000 were discussed by using different characterization techniques such as TEM, EDX, UV–Vis, DLS, ICP-MS and FTIR spectroscopic techniques.

Experimental Work

Materials

Au(III) acetate [Au $(CH_3COO)_3$, Alfa Aesar, 99.9%], Hydrochloric acid (HCl, 30% concentrated), Sodium Hydroxide (NaOH, concentration of 40 g/mol in pellets), Sodium carbonate anhydrous (Na_2CO_3, Applichem Panreac), PEG-5000 (Alfa Aesar), De-ionized water (purified with the Millipore system).

Thermal Analysis of the Decomposition of Gold(III) Acetate

Experiments of TGA-DT were performed to evaluate the temperature of decomposition of Au(III) acetate upon heating. This analysis has helped in the interpretation about the chemical and physical processes which occurred in the evaporation zone and reaction zone in USP during the synthesis mechanism of AuNPs while using Au(III) acetate as a reactant precursor. The evaporation and reaction zone temperatures were taken in accordance with the thermal decomposition range of Au(III) acetate. The initial steps in the decomposition process and mass loss are critical in determining the final characteristics of the AuNPs.

The decomposition behavior of Au(III) acetate was studied using TGA-DT analysis in TA instruments Q50. The following initial parameters were taken for the analysis: Au(III) acetate: 3 mg, inert gas: N_2, gas flow rate: 100 ml/min, heating rate: 5 °C/min, temperature range: 25–250 °C. Figure 1 show the thermogravimetric data at heating rate of 5 °C/min for Au(III) acetate mass loss under heating, and the derivative of the percent mass loss with respect to temperature. The decomposition of Au(III) acetate starts at about 85 °C while the significant mass loss was observed between 140 and 200 °C with 30% of the average peak mass rate of loss occurring at T = 160 °C. The TGA peak was located in the temperature range between 140 and 210 °C using a heating rate of 5°C min^{-1} where the thermal

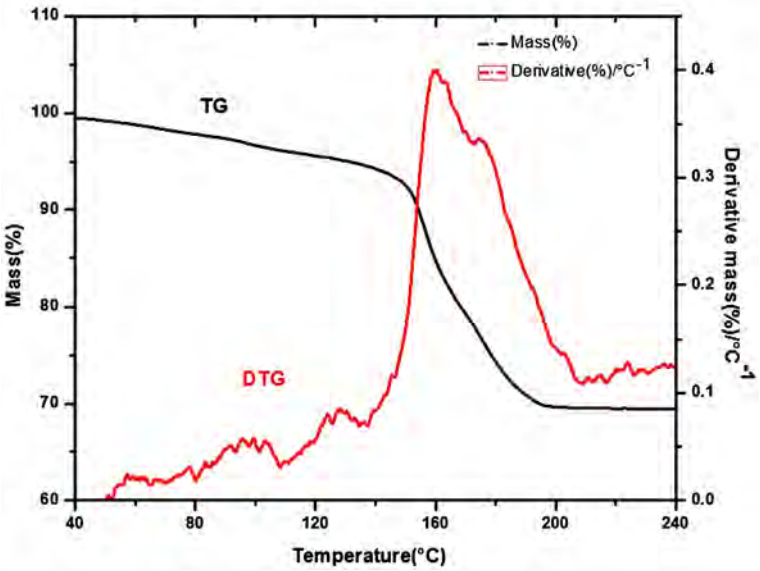

Fig. 1 TG and DT curve for Au(III) acetate in nitrogen using a heating rate of 5 °C/min

decomposition of the Au(III) acetate occurred. Therefore, in order to promote the evaporation of the aerosol droplets and the chemical reactions for the nucleation and growth of the AuNPs, the evaporation zone and reaction zone temperature was taken as 100 and 300 °C respectively.

USP Equipment

The series of experiments for the synthesis of AuNPs were carried out on the modular USP device at the IME Institute of Process Metallurgy and Metal Recycling, RWTH Aachen, Germany (Fig. 2). The device contained the following main parts: ultrasonic generator, heating chambers, collection bottles and transport tubes. This modular USP device was redesigned to modular separate heating zones in order to divide the two important stages of heating into aerosol droplet evaporation in the evaporation zone and particle drying in the reaction zone, maintained at different temperatures T_1 and T_2 °C respectively. The ultrasonic aerosol generator (Gapusol, RBI France with piezoelectric transducer membrane frequency of 1.6 MHz using intensity to 9) was used for the generation of precursor aerosol droplets. These aerosol droplets were transported through a quartz tube (length = 28 cm and diameter = 2 cm) to the heating zones of the equipment. Dry Nitrogen (N_2, 99.9%) was used as the carrier gas with a flow rate of 2 l/min, while Hydrogen gas (H_2, 99.9%) was used for the reduction of the aerosol droplets of the precursor solution into AuNPs, which was fed directly into the Chamber-II at a flow rate of 1 l/min. The collection bottles contained 250 ml of de-ionized water mixed with 0.6 gm of PEG-5000.

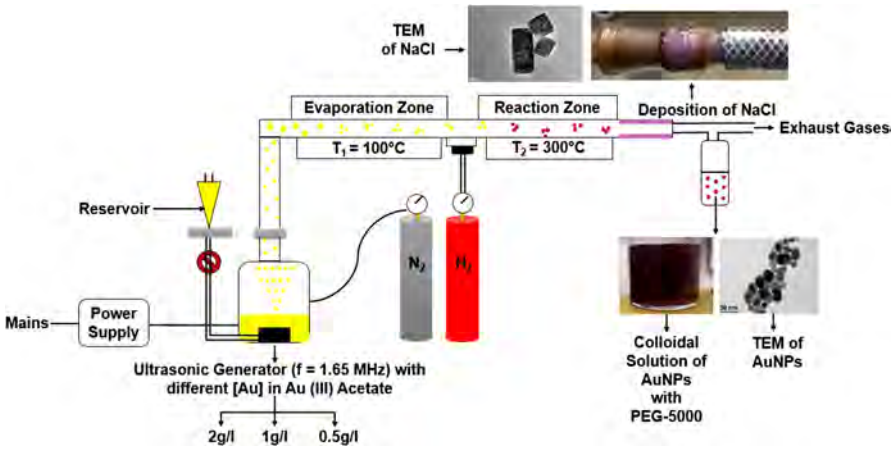

Fig. 2 Schematic diagram of experimental setup of ultrasonic spray pyrolysis comprising of ultrasonic generator, evaporation chamber, reaction chamber, quartz transport tubes and collection bottles for AuNPs

Synthesis and Current Issues Faced in the Synthesis of AuNPs with USP

Method of Preparation of the Precursor Solution

The in-received Au(III) acetate powder was dark brown in color containing micron sized particles. Water was added to the Au(III) acetate powder of [Au] = 4 g/l and was stirred magnetically and heated. Since its solubility in the water was low, therefore, insoluble particles of the powder became settled down in the container as shown in Fig. 3a. The partially insoluble aqueous solution of Au(III) acetate was tested with a series of trial experiments run as USP Trial Run 1 in the USP equipment for the synthesis of AuNPs.

USP Trial Run 1 The following initial parameters were taken: frequency = 1.65 MHz, intensity = 8, ambient temperature = 21 °C. N_2 gas flow rate = 2 l/min (Table 1).

The final collection bottles showed a transparent solution which was very similar to the initial solution of PEG-5000, thereby implying no formation of AuNPs. This may be due to the partially insoluble Au(III) acetate in water. Therefore, to make a soluble solution of Au(III) acetate, 5 ml of the insoluble solution of Au(III) acetate was mixed with HCl and HNO_3 in separate containers (Fig. 3b, c). A clear yellow solution was obtained with the addition of HCl in the solution, while it remained undissolved with HNO_3. The obtained clear solution with HCl was tested again with a second series of trials, run as USP Trial Run 2 in USP for the synthesis of AuNPs.

USP Trial Run 2 100 ml HCl was mixed into an Au(III) acetate solution (400 ml) having 4 g/l [Au] and was stirred magnetically (Fig. 3c). The following parameters were taken in the USP equipment: frequency = 1.65 MHz, intensity = 9, ambient

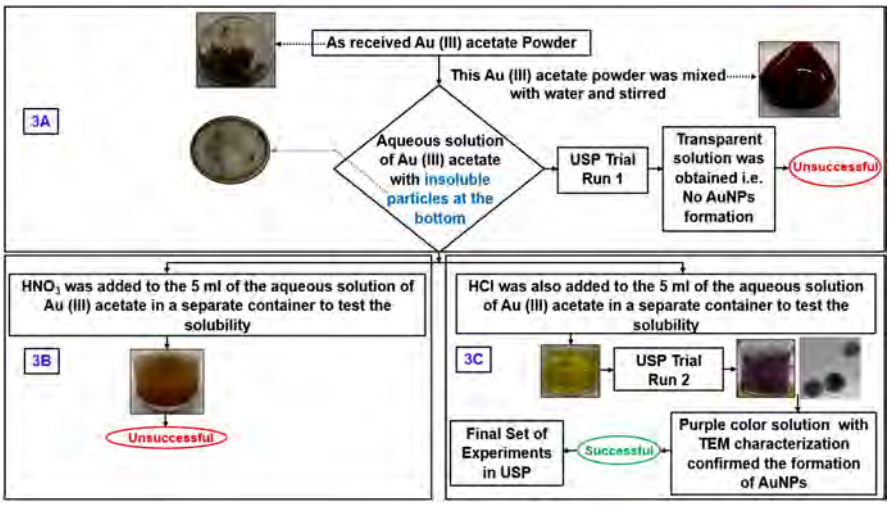

Fig. 3 Flow chart of the procedure followed in the preparation of the precursor solution of Au(III) acetate comprising: **a** initial trial of aqueous solution of Au(III) acetate with USP, **b** unsuccessful testing of the solubility of Au(III) acetate with HNO_3, **c** successful testing of the solubility of Au(III) acetate with HCl and synthesizing AuNPs through USP with the obtained solution, followed by the final set of experiments

Table 1 Parameters considered in USP such as concentration of the Au in Au(III) acetate precursor, evaporation zone temperature (T_1), reaction zone temperature (T_2), gas flow rate of N_2 and duration of the experiment for the synthesis of AuNPs during *USP Trial Run 1* were mentioned

[Au] (g/l)	T_1 (°C)	T_2 (°C)	N_2 (l/min)	Duration of experiment (h)
0.5	100	400	2.0	3

Table 2 Parameters with an addition of H_2 gas flow rate taken for the synthesis of AuNPs during *USP Trial Run 2* were mentioned

[Au] (g/l)	T_1 (°C)	T_2 (°C)	N_2 (l/min)	H_2 (l/min)	Duration of experiment (h)
4	100	300	2.0	1	3

temperature = 21 °C. Additionally, hydrogen (H_2, 99.9%) gas flow rate = 1 l/min (Table 2).

The collection bottles showed a purple colloidal solution, indicating the formation of AuNPs. Since, the acidic value of these AuNP was very high (about pH value range of 1–2) due to the addition of HCl. Therefore, sodium hydroxide (NaOH) in pellet forms and sodium carbonate anhydrous in powder form had been

added to the Au(III) acetate solution with HCl of [Au] of 2 g/l. The pH value of the precursor solution was increased to the desired range of 6–7.

Final set of experiments The final set of experiments were carried out with the precursor solution of Au(III) acetate mixed with HCl, NaOH and Na_2CO_3 which was tried successfully in USP Trial Run 2. The temperature of the evaporation chamber was kept at 100 °C and the reaction chamber was maintained constantly at 300 °C. Therefore, the concentrations of the Au in the Au(III) acetate solution were varied as 2, 1 and 0.5 g/l. The collection bottles contained PEG-5000 mixed in water. The parameters taken for the final set of experiments are shown in Table 3.

Characterization of Gold Nanoparticles

TEM and EDX

Morphology with the crystal structure of the AuNPs was investigated by conventional transmission electron microscopy (CTEM; JEOL 2100), high resolution transmission electron microscopy (HRTEM; JEOL 2100), electron diffraction (ED/TEM; JEOL 2100), electron dispersive spectroscopy (EDS/TEM; JED 2300). A drop of colloidal suspension of AuNPs with PEG-5000 was pipetted onto a formvar film coated with a layer of carbon, or a lacey formvar film coated with a layer of carbon, or a lacey formvar film enforced by a heavy coating of carbon TEM copper grid of 200 mesh and dried at room temperature. The grid was then observed directly in a TEM once the medium evaporated.

UV–Vis Spectrometry

UV–Vis spectra were run in a colloidal solution of AuNPs with PEG by using quartz cells, with a Varian Cary 100 Scan—UV–Vis spectrophotometer.

FTIR

The PEG-AuNPs colloidal solutions were condensed by combining centrifugation and solvent evaporation under reduced pressure. The centrifugation was performed with a Hettich Zentrifugen Rotina 380R, Germany and an Amicon Ultra 15,

Table 3 Final set of experiments in the USP with varying concentration of Au in Au(III) acetate along with other parameters

Exp. no.	Variable parameter	Solution	[Au] (g/l)	T_1 (°C)	T_2 (°C)	N_2 (l/min)	H_2 (l/min)
1	Concentration	Au.ac + HCl + NaOH + Na_2CO_3	2	100	300	2	1
2		Au.ac + HCl + NaOH + Na_2CO_3	1	100	300	2	1
3		Au.ac + HCl + NaOH + Na_2CO_3	0.5	100	300	2	1

Millipore, US centrifugal filter at 4 °C. The centrifugation took place at 3200*g* for 30 min. The PEG-AuNPs were condensed further into powder form by Mini Lyotrap Freeze Dryers, LTE Scientific, United Kingdom for 24 h. The obtained powder was subjected to FTIR measurements carried out on a Perkin Elmer Spectrum GX spectrometer. The ATR accessory (supplied by Specac Ltd., UK) contained a diamond crystal. All spectra (16 scans at 4 cm^{-1} resolution and rationed to the appropriate background spectrum) were recorded at 298 K over a wavenumber range of 500–4000 cm^{-1}.

ICP MS Measurements

An ICP MS was used for the Au^{3+} quantification (i.e. concentration of Au in AuNPs). Prior to the analysis, samples were diluted tenfold with de-ionized Milli-Q water (purity 18 MΩ cm) and acidified with aqua regia (5% v/v). For calibration, single element standard solutions (Merck, Darmstadt, Germany) were used. Analysis was carried out using an ICP MS spectrometer (Agilent, 7500 ce, equipped with collision cell) under the operating conditions: RF power—1.5 kW, sample depth 8 mm, Nebulizer–Meinhard, plasma gas flow (l/min)—15, Nebulizer gas flow (l/min)—0.85, make up gas flow (l/min)—0.28, reaction gas flow (ml/min)—4.0.

Zeta Potential Measurements

Zeta potential was measured by using Malvern Zetasizer Nano ZS apparatus (Malvern Zetasizer Nanoseries Instruments Ltd., Worcestershire, UK) with disposable folded capillary cuvettes provided with electrodes.

Statistics and Diagrams

Data were presented as a representative experiment or as a mean ± standard deviation (SD) of at least 3 independent experiments. The differences between control experimental samples were analyzed using the Kruskal–Wallis test with Bonferoni post test and values at $p < 0.05$ or less were considered to be statistically significant. Origin Pro 8 was used for plotting the graphs and figures were made with the help of Microsoft Office Tools.

Measurement of Size and Circularity Through TEM

The size and circularity measurements of AuNPs were done with the help of TEM images in the following mentioned procedure. A minimum of 200 discrete AuNPs were measured from each of widely separated regions of the two samples to measure the size and circularity of the AuNPs from TEM images according to Standard ISO 13322-1:2004. An ImageJ software tool was used for the data analysis algorithm.

Results and Discussion

TEM with Size Distribution of AuNPs

TEM confirmed the presence of the AuNPs synthesized at different concentrations of [Au] in Au(III) acetate of 2, 1 and 0.5 g/l as shown in Fig. 4a–c. These AuNPs were more about circular in shape with no visible defects such as cracks, porosity and pin holes etc. Also, the density of the AuNPs looked to be uniform and similar

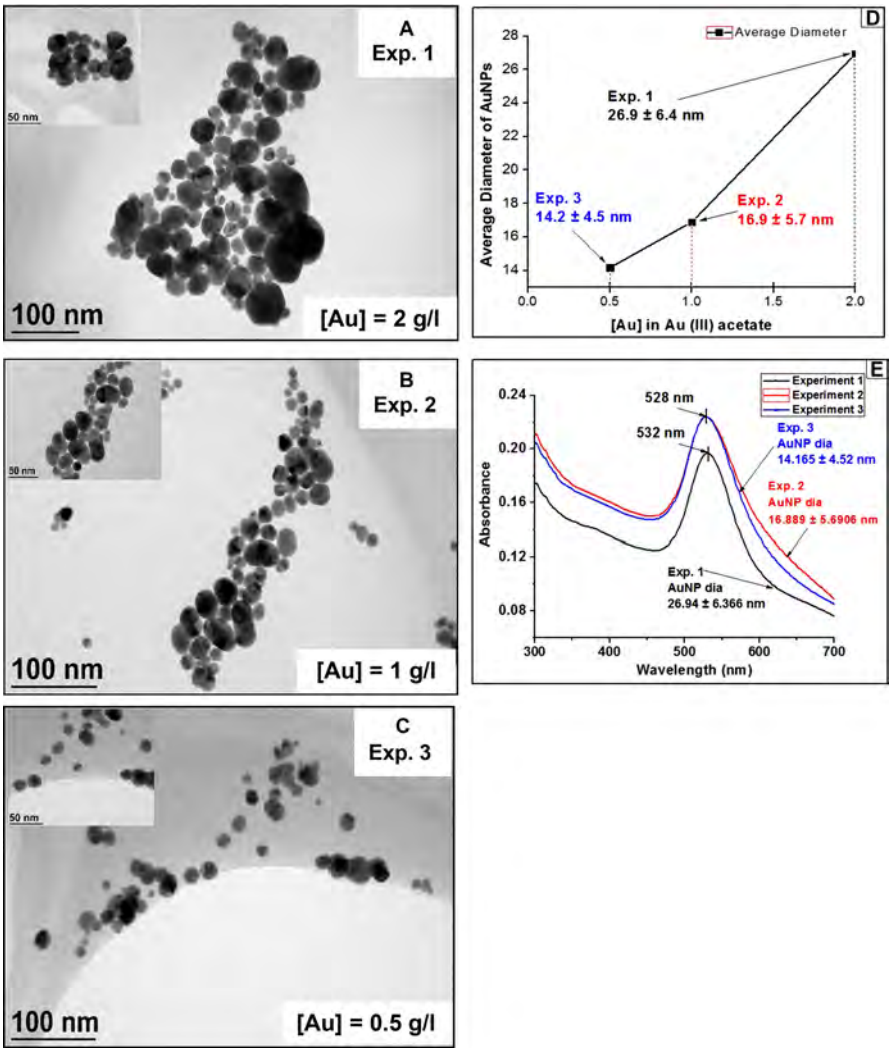

Fig. 4 **a–c** The TEM images of the AuNPs synthesized from Exp. 1, 2 and 3 respectively. **d** The size distribution of AuNPs obtained by TEM characterization and **e** UV–Vis measurement of the AuNPs from Exp. 1, 2 and 3 respectively

for all the AuNPs. A small section of the AuNPs were coalesced due to the phenomena of agglomeration, while the majority of them remained unagglomerated.

The average mean diameters with standard deviation (SD) of the AuNPs measured in Experiments 1, 2 and 3 from TEM images were 26.90 ± 6.40, 16.90 ± 5.70 and 14.20 ± 4.50 nm respectively. These measurements of mean sizes showed that, with increasing [Au] in the Au(III) acetate precursor solution, AuNPs sizes increased, and vice versa (Fig. 4d). The calculated mean value with SD of circularity of AuNPs in accordance to ISO 13322-1:2004 for the Exp. 1, 2 and 3 were 0.91 ± 0.04, 0.88 ± 0.02 and 0.86 ± 0.03 respectively (with 0–1 range, 0 signifies an irregular shape and 1 signifies a perfect circle). These values showed that these particles were more about circular in shape.

UV–Vis Measurement

UV–Vis absorption spectroscopy is one of the key techniques to evaluate the structural, as well as the optical properties of AuNPs, because the adsorption bands relate the precise diameter and aspect ratio of AuNPs. In the colloidal AuNPs of nano-size range, the surface electron cloud can vibrate and absorb the electromagnetic radiation of a particular energy. Therefore, these AuNPs obtained through USP were observed in the UV–Vis visible spectrum to analyze the size effect of AuNPs on the surface plasmon resonance (SPR) [68].

The UV–Vis measurement of AuNPs with PEG at a pH range of 6–7 showed an absorption at $\sim$528 nm of AuNPs obtained from Exp. 2 and 3 and at $\sim$532 nm of AuNPs from Exp. 1 (Fig. 4e). This adsorption wavelength value signifies the peculiar characteristics of the localized SPR peak of Au colloids [69, 70]. This SPR peak formation in the UV–Vis spectra was, basically, due to the light scattering caused by the colloidal solution of AuNPs, and the peak positions attained at the maximum spectra value were because of the absence of the large agglomeration between the AuNPs obtained through the USP process. These curves also seemed to be symmetric and narrow in nature, indicating the presence of a smaller average particle size and mono-disperse size range of AuNPs. There was a small shift of the SPR peak from 528 to 532 nm due to the increasing [Au] in the Au(III) acetate solution from 0.5 to 2.0 g/l. This increase in the plasmon absorption of the AuNPs can be attributed to the increasing concentration of [Au] in the precursor solution leading to the increase of AuNPs dia's.

EDX Characterization

Figure 5a shows a TEM image of an agglomerated AuNP which was formed from a small cluster of AuNPs. The crystal structure of this AuNP was polycrystalline, which was metallic in nature. Figure 5b, c show an Electron diffraction pattern simulation of the corresponding AuNP describing an Fm-3m space group which corresponds to the FCC lattice structure (Fig. 5d). This FCC lattice structure had surface energies in the following order $a_{\{111\}} < a_{\{100\}} < a_{\{110\}}$.

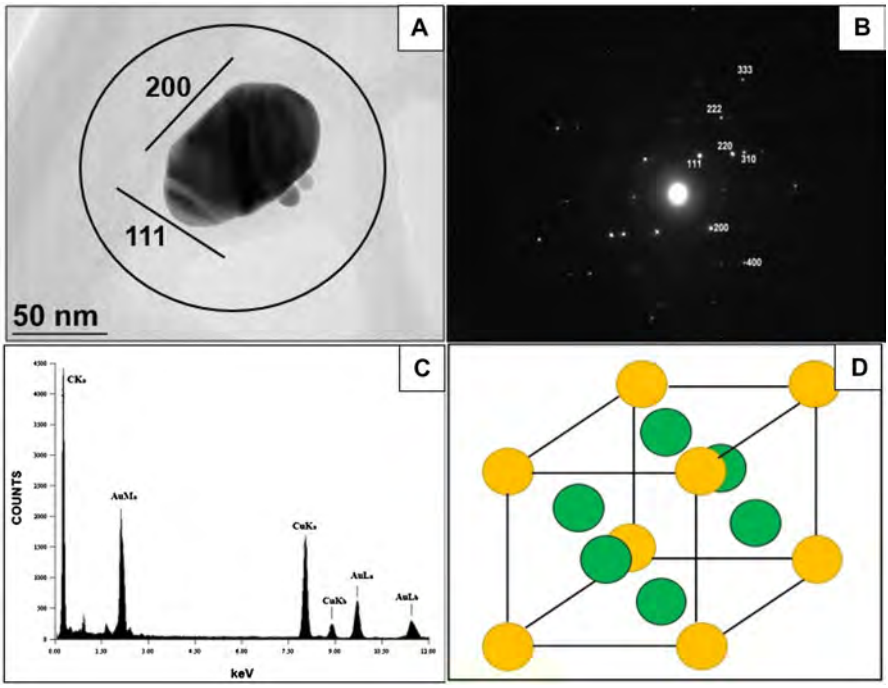

Fig. 5 Electron diffraction on the synthesized singular AuNP with a crystal lattice simulation: **a** TEM image of a single AuNP with visible selected site of electron diffraction, **b** electron diffraction of AuNPs, **c** EDX spectra, **d** face centered cubic lattice structure simulation

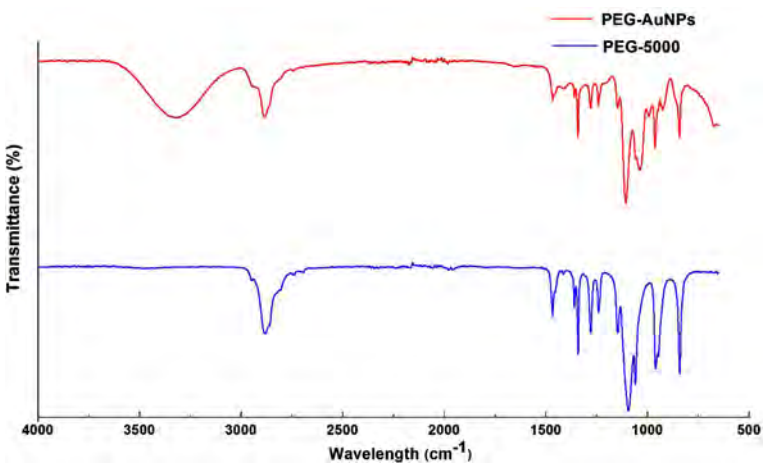

Fig. 6 FTIR spectra of synthesized PEG-AuNPs

FTIR Analysis

FTIR analysis confirmed the PEG-capping on the surface of AuNPs as shown in Fig. 6. The FTIR spectrum of PEG coated AuNPs was similar to that of the original PEG-5000, although the differences were observed in the slight shift of wavenumber. The FTIR spectrum of PEG-AuNPs was in good agreement with that reported by Joanne and Seung Kwon Seol [55, 63, 68]. Absorbance peaks were present in the spectrum of PEG-AuNPs and these peaks are assigned as follows: 3317–2883 cm^{-1} (–CH_2 stretching), 1342 cm^{-1} (C–H bending, –CH_2 and –CH_3), 1105 cm^{-1}(C–O–C stretching) and 963–672 (N–H wagging). These peaks were consistent with the spectrum of pure PEG-5000, indicating the adsorption of PEG molecules onto the surface of AuNPs.

ICP-MS Analysis

The final concentration of AuNPs obtained at varying concentrations of initial precursor solution of Au(III) acetate at 2, 1 and 0.5 g/l were 29, 34 and 79 ppm respectively (Table 4). With lower concentration of precursor solution of Au(III) acetate, higher concentration of AuNPs were obtained and vice versa. This may be due to the following possible losses of large AuNPs agglomerates in the synthesis mechanism: (1) since higher concentration of the precursor solution had produced larger sizes of AuNPs agglomerates that flowed along the heating chambers, due to which their agglomerate size increased to such a large extent that some of them settled down along the reactor walls via sedimentation. Theoretically, the mass of one AuNP calculated at the highest concentration to lowest concentration of the precursor solution decreased from 0.2 to 0.05 to 0.02 fg. The force needed to carry the higher mass of AuNPs was just not sufficient to pass through the heating chambers to the collections bottles, thereby falling in-between the transport tubes. This may increase the rate of sedimentation at the higher concentration. (2) The other larger AuNPs agglomerates, along with the by-product sodium chloride near the reactor wall downstream of the heat front, experienced strong temperature gradients, forcing them to deposit in the powder form. (3) Other particles also ended up at the reactor walls by means of turbulent eddies due to the injection of hydrogen gas before the second heating zone and stuck to the quartz transport tubes [71]. Therefore, kinetic control of parameters were very important to achieve a higher concentration of obtained AuNPs to minimize these kinetic losses.

Zeta Potential Measurement

The zeta potential of AuNPs from Exp. 1, 2 and 3 were -22.2 ± 1.8, -19.6 ± 2.3 and -23.3 ± 1.4 mV respectively. These negatively charged nanoparticles can repel each other more effectively, allowing the PEG molecules to cover them before contact occurs. These kinetic considerations are expected to limit the coalescence of the forming clusters, leading to smaller AuNPs [72, 73].

Table 4 Results of the AuNPs dia by TEM characterization, concentration of AuNPs by ICP-MS measurements, surface zeta potential by DLS technique

Exp. no.	Precursor solution	[Au] (g/l)	Size measurements by TEM (nm)	Theoretical mass of one AuNP (fg)	Zeta potential (mV)	[Au] of AuNPs by ICP-MS (ppm)
1	Au.ac + HCl + NaOH + Na_2CO_3	2	26.9 ± 6.4	0.2	−22.2 ± 1.8	29
2	Au.ac + HCl + NaOH + Na_2CO_3	1	16.9 ± 5.7	0.05	−19.6 ± 2.3	34
3	Au.ac + HCl + NaOH + Na_2CO_3	0.5	14.2 ± 4.5	0.02	−23.3 ± 1.4	79

Chemical Reactions Involved in the USP

The possible chemical reactions for the synthesis mechanism of AuNPs with Au(III) acetate are mentioned below. Initially, the Au(III) acetate powder with low solubility was mixed with water to form an aqueous solution of Au(III) acetate as shown in Eq. 1.

$$Au(CH_3COO)_3 + H_2O = Au(CH_3COO)_3 \cdot 3H_2O \quad (1)$$

In the second step of this synthesis process, HCl with NaOH and Na_2CO_3 was added to the aqueous solution of Au(III) acetate to obtain a clear and fully soluble precursor solution as described in Eq. 2. The aerosol droplets of the solution were first heated in the evaporation zone and then with H_2 gas in the reaction zone to produce pure AuNPs with the sedimentation of sodium chloride salt in the transport tubes as investigated by TEM. Acetic acid was the dominant organic by-product with CO_2 bubbles formed in the solution [25]. These chemical equations were reported evidence by the experimental products formed.

$$\begin{aligned} &Au(CH_3COO)_3 \cdot 3H_2O + HCl + NaOH + Na_2CO_3 + H_2 \\ &\quad = Au + NaCl + CH_3COOH + 2CH_3COONa + 5H_2O + CO_2 \end{aligned} \quad (2)$$

Conclusions

This work provides the first documentation of the synthesis and the issues faced with potential solutions that synthesizing AuNPs with a precursor solution of Au(III) acetate solution with varying concentrations through USP was possible. The TGA-DT analysis of Au(III) acetate provided the key information for thermal decomposition temperature and mass loss percent in the temperature range of 100−300 °C. TEM and UV–Vis measurement confirmed the synthesis of circularly shaped, largely unagglomerated AuNPs with no physical defects. FTIR analysis also confirmed the capping of PEG on the surface of AuNPs. Size measurements of AuNPs showed that the diameters of AuNPs increases with the increasing [Au] in the Au(III) acetate precursor solution. With the ICP-MS measurements, it can be concluded that the lower the concentration of the Au(III) acetate, the higher the concentration of AuNPs obtained, and vice versa, due to the sedimentation and turbulent losses of larger AuNPs in the transport tubes. The work provides key insights into the physical and chemical pathways that are important during the synthesis of AuNPs with Au(III) acetate and provides qualitative data that will be critical for controlled synthesis.

Acknowledgements The study was supported by the European Union—Erasmus Mundus Action 2 Lot 13 Euphrates Program and Slovenian Research Agency ARRS Slovenia (P2-120 and Martina Program). Many thanks to Dr.Vanja Kokol, Dr. Irena Ban and Mrs. Vera Vivod for helping in the UV–Vis spectroscopy, TGA and FTIR analysis.

Compliance with Ethical Standards

Conflict of interest All the authors declared that there is no conflict of interest.

References

1. B. Sepúlveda, P. C. Angelomé, L. M. Lechuga, and L. M. Liz-Marzán (2009). *Nano Today* **4**, (3), 244–251.
2. K. M. Mayer and J. H. Hafner (2011). *Chemical Reviews* **111**, (6), 3828–3857.
3. K. Saha, S. S. Agasti, C. Kim, X. Li, and V. M. Rotello (2012). *Chemical Reviews* **112**, (5), 2739–2779.
4. J. Z. Zhang *Optical Properties and Spectroscopy of Nanomaterials*, 1st ed (World Scientific Publishing Company, Singapore, 2009).
5. P. Alivisatos (2004). *Nature Biotechnology* **22**, 47–52.
6. J. L. West and N. J. Halas (2000). *Current Opinion in Biotechnology* **11**, 215–217.
7. I. K. Ding, J. Zhu, W. Cai, et al. (2011). *Advanced Energy Materials* **1**, (1), 52–57.
8. D. Wu, X. Xu, and X. Liu (2008). *The Journal of Chemical Physics* **129**, 074313.
9. A. Lahde, I. Koshevoy, T. Karhunen, T. Torvela, T. A. Pakkanen, and J. Jokiniemi (2014). *Journal of Nanoparticle Research*. doi:10.1007/s11051-014-2716-4.
10. O. Masala and R. Seshadri (2004). *Annual Review of Materials Research* **34**, 41–81.
11. M. Brust and C. J. Kiely (2002). *Colloids and Surfaces* **202**, 175–186.
12. Y. Yin, C. Erdonmez, S. Aloni, and A. P. Alivisatos (2006). *Journal of the American Chemical Society* **128**, 12671–12673.
13. N. Bao, L. Shen, Y. Wang, P. Padhan, and A. Gupta (2007). *Journal of the American Chemical Society* **129**, 12374–12375.
14. H. Hiramatsu and F. E. Osterloh (2004). *Chemistry of Materials* **16**, 2509–2511.
15. S. Sun, B. C. Murray, D. Weller, L. Folks, and A. Moser (2000). *Science* **287**, 1989–1992.
16. S. Sun and H. Zeng (2002). *Journal of the American Chemical Society* **124**, 8204–8205.
17. M. Haruta, S. Tsubota, T. Kobayashi, H. Kageyama, M. J. Genet, and B. Delmon (1993). *Journal of Catalysis* **144**, 175–192.
18. S. Ivanova, V. Pitchon, Y. Zimmermann, and C. Petit (2006). *Applied Catalysis, A: General* **298**, 57–64.
19. M. Bowker, A. Nuhu, and J. Soares (2007). *Catalysis Today* **122**, 245–247.
20. J. D. Lessard, I. Valsamakis, and M. Flytzani-Stephanopoulos (2012). *Chemical Communications* **48**, 4857–4859.
21. A. Hugon, N. E. L. Kolli, and C. Louis (2010). *Journal of Catalysis* **274**, 239–250.
22. X. Lu, H. Y. Tuan, B. A. Korgel, and Y. Xia (2008). *Chemistry–A European Journal* **14**, 1584–1591.
23. A. Lahde, I. Koshevoy, T. Karhunen, T. Torvela, T. A. Pakkanen, and J. Jokiniemi (2014). *Journal of Nanoparticle Research*. doi:10.1007/s1105101427164.
24. M. Garza, I. López, and I. Gómez (2013). *Advances in Materials Science and Engineering* **916908**, 1–5.
25. S. D. Bakrania, G. K. Rathore, and M. S. Wooldridge (2009). *Journal of Thermal Analysis and Calorimetry* **95**, (1), 117–122.
26. H. Sakurai, K. Koga, Y. Iizuka, and M. Kiuchia (2013). *Applied Catalysis, A: General* **462–463**, 236–246.
27. M. T. Htay, Y. Hashimoto, N. Momose, and K. Ito (2009). *Journal of Crystal Growth* **311**, (20), 4499–4504.
28. M. A. Montero, M. R. G. Chialvo, and A. C. Chialvo (2009). *Journal of Materials Chemistry* **19**, (20), 3276–3280.
29. U. Alver, T. Kılınç, E. Bacaksiz, and S. Nezir (2007). *Materials Chemistry and Physics* **106**, (2–3), 227–230.
30. H. Zhang and M. T. Swihart (2007). *Chemistry of Materials* **19**, (6), 1290–1301.
31. S. E. Skrabalak and K. S. Suslick (2005). *Journal of the American Chemical Society* **127**, (28), 9990–9991.

32. P. Majerič, R. Rudolf, I. Anžel, J. Bogović, S. Stopić, and B. Friedrich (2015). *Materials Technology* **49**, (1), 75–80.
33. D. Mott, et al. (2009). *Chemistry of Materials* **22**, 261–271.
34. D. Mott, J. Galkowski, L. Wang, J. Luo, and J. C. Zhong (2007). *Langmuir* **23**, 5740–5745.
35. Z. Xu, C. Shen, Y. Hou, H. Gao, and S. Sun (2009). *Chemistry of Materials* **21**, 1778–1780.
36. S. D. Bakrania, T. A. Miller, C. Perez, and M. S. Wooldridge (2007). *Combustion and Flame* **148**, 76.
37. S. D. Bakrania, C. Perez, and M. S. Wooldridge (2007). *Proceedings of the Combustion Institute* **31**, (II), 1797–1804.
38. L. Mangolini, E. Thimsen, and U. Kortshagen (2005). *Nano Letters* **5**, (4), 655.
39. E. Thimsen and P. Biswas (2005). *AIChE Journal* **53**, (7), 1727.
40. E. Thimsen, N. Rastgar, and P. Biswas (2005). *Journal of Physical Chemistry* **112**, (11), 4134.
41. P. Biswas and E. Thimsen *Aerosol Measurements*, 3rd ed (Wiley-VCH, New York, 2011). **(Chapter 33)**.
42. R. Rudolf, B. Friedrich, S. Stopic, I. Anzel, S. Tomic, and M. Colic (2012). *Journal of Biomaterials Applications* **26**, 595–612.
43. J. Dokic, R. Rudolf, S. Tomic, S. Stopic, B. Friedrich, B. Budic, I. Anzel, and M. Colic (2012). *Journal of Biomedical Nanotechnology* **8**, 528–538.
44. M. Afzal, P. K. Butt, and H. Ahmad (1991). *Journal of Thermal Analysis* **37**, 1015.
45. S. Stopic, R. Rudolf, J. Bogovic, P. Majeric, M. Colic, S. Tomic, M. Jenko, and B. Friedrich (2013). *MTAEC9* **47**, (5), 557–583.
46. S. Stopic, B. Friedrich, H. U. Fritsching, K. Raic, Synthesis of metallic nanosized particles by ultrasonic spray pyrolysis, *IME Metallurgische Prozesstechnik and Metallrecycling, RWTH Aachen, Germany*, 1st ed (Shaker Verlag, 2015).
47. P. Majeric, D. Jenko, B. Budic, S. Tomic, M. Colic, B. Friedrich, and R. Rudolf (2015). *Nanoscience and Nanotechnology Letters* **7**, 1–10.
48. P. Majerič, B. Friedrich, and R. Rudolf (2015). *Materials Technology* **49**, (1), 791–796.
49. R. Rudolf, P. Majeric, S. Tomic, M. Shariq, U. Fercec, B. Budic, B. Friedrich, D. Vucevic, M. Colic, *Journal of Nanomaterials* (2017). doi:10.1155/2017/9365012.
50. A. Barreto, L. G. Luis, A. V. Girao, T. Trindade, M. Amadeu, V. M. Soares, and M. Oliveira (2015). *Journal of Nanoparticle Research*. doi:10.1007/s1105101533020.
51. S. C. Tsai, Y. L. Song, C. S. Tsai, C. C. Yang, W. Y. Chiu, and H. M. Lin (2004). *Journal of Materials Science* **39**, 3647–3657.
52. T. Niidome, M. Yamagata, Y. Okamoto, et al. (2006). *Journal of Controlled Release* **114**, (3), 343–347.
53. D. K. Kim, S. J. Park, J. H. Lee, Y. Y. Jeong, and S. Y. Jon (2007). *Journal of the American Chemical Society* **129**, (24), 7661–7665.
54. C. J. Liu, C. H. Wang, C. C. Chien, et al. (2008). *Nanotechnology* **19**, 29.
55. S. K. Seol, D. Kim, S. Jung, W. S. Chang, and J. T. Kim (2013). *Journal of Nanomaterials*. doi:10.1155/2013/531760.
56. B. D. Warheit (2008). *Toxicological Sciences* **101**, 183–185.
57. L. Canesi, C. Ciacci, R. Fabbri, A. Marcomini, G. Pojana, and G. Gallo (2012). *Marine Environment Research* **76**, 16–21.
58. A. L. Fernandez, A. Fernandez, and J. Blasco (2012). *TrAC Trends in Analytical Chemistry* **32**, 40–59.
59. T. B. Lee and F. J. Ranville (2012). *Journal of Hazardous Materials* **213–214**, 434–439.
60. S. Balog, L. R. Lorenzo, A. C. Monnier, M. R. Obiols, B. R. Rothen, P. Schurtenberger, and A. F. Petri (2015). *Nanoscale* **7**, 5991–5997.
61. Y. Liu, K. M. Shipton, J. Ryan, D. E. Kaufman, S. Franzen, and L. D. Feldheim (2007). *Analytical Chemistry* **79**, 2221–2229.
62. V. J. Jokerst, T. Lobovkina, N. R. Zare, and S. S. Gambhir (2011). *Nanomedicine* **6**, 715–728.
63. J. Manson, D. Kumar, B. Meenan, and D. Dixon (2011). *Gold Bulletin* **44**, 99–105.
64. L. H. T. Nghiem, T. T. Nguyen, E. Fort, P. T. Nguyen, N. M. T. Hoang, Q. T. Nguyen, and N. H. Tran (2012). *Advances in Natural Sciences* **3**, 015002.
65. C. N. R. Rao, G. U. Kulkarni, P. J. Thomas, and P. P. Edwards (2000). *Chemical Society Reviews* **29**, 27.
66. H. Bonnemann and R. M. Richards (2001). *European Journal of Inorganic Chemistry* **1434**, 2455–2480.
67. X. Sun, S. Dong, and E. Wang (2006). *Materials Chemistry and Physics* **96**, 29–33.

68. N. Srivastava and M. Mukhopadhyay (2015). *Journal of Cluster Science*. doi:10.1007/s10876-014-0726-0.
69. N. Saha and S. D. Gupta (2016). *Journal of Cluster Science*. doi:10.1007/s10876-016-1009-8.
70. A. Parveen and S. Rao (2015). *Journal of Cluster Science*. doi:10.1007/s10876-014-0813-2.
71. T. T. Kodas and M. H. Smith *Aerosol Processing of Materials*, 1st ed (Wiley-VCH, New York, 1999), pp. 45–74.
72. J. P. Sylvestre, A. V. Kabashin, E. Sacher, and J. H. T. Luong (2004). *Journal of the American Chemical Society*. doi:10.1021/ja048678s.
73. G. Cardenas, V. Saez, and C. Cruzat (2015). *Journal of Cluster Science*. doi:10.1007/s10876-016-1071-2.